

Selectivity of nanoporous MnO₂ and TiO₂ membranes for residual contaminants in treated wastewater

A. Giwa^{a,†}, S.M. Jung^{b,†}, M. Ahmed^c, W. Fang^d, J. Kong^{e,§}, S.W. Hasan^{f,§}

^{a,c,f} Department of Chemical Engineering, Khalifa University of Science and Technology, Masdar City campus, P.O. Box 54224, Abu Dhabi, United Arab Emirates

^{b,d,e} Department of Electrical Engineering and Computer Science at Massachusetts Institute of Technology, Cambridge, Massachusetts 02139, USA

Corresponding authors: ^{f,§} swajih@masdar.ac.ae, Tel: +971 2 810 9237 (S.W. Hasan)

^{e,§} jingkong@mit.edu, Tel: +1 617 324 4068 (J. Kong)

Abstract

Treated effluent from an electrically-enhanced membrane bioreactor (eMBR) was filtered through MnO₂ or TiO₂ nanoporous membranes for the removal of residual heavy metals, bacteria and biological oxygen demand (BOD). The fresh and spent membranes were characterized via energy-dispersive X-ray spectroscopy (EDAX), zeta potential analysis and thermogravimetric analysis (TGA). Water analysis was obtained via UV/Vis spectrophotometry. For most contaminants, eMBR-TiO₂ showed highest removal efficiency than MnO₂ because of the combined adhesion and photocatalytic effects of TiO₂, i.e. 100% bacteria, 97.8% BOD, and 96.9% Zn removal by eMBR-TiO₂ as compared to 97.5% bacteria, 97.6% BOD, and 80% Zn removal by eMBR-MnO₂. Meanwhile, eMBR-MnO₂ showed higher removal efficiency for Fe, i.e. 97.9% as compared to 81.1% by eMBR-TiO₂.

Keywords: MnO₂, TiO₂, electrically-enhanced MBR, nanowires, wastewater treatment.

1. Introduction

Several technologies have been used for wastewater treatment such as biological processes (activated sludge processes (ASPs), aerated lagoons, trickling filters, etc.), membrane filtration (membrane bioreactors (MBRs), nano-enhanced membrane filters, etc.), and electrocoagulation (EC) [1–3]. Each process has some deficiencies. ASPs are simple to start-up and operate, and require low capital and operating costs. However, they produce huge amounts of sludge, are slow to adapt to environmental fluctuations, and are highly dependent on settling requirements [4,5]. Aerated lagoons and constructed wetlands are known to be cost effective in areas where land is inexpensive. They are simple to operate and efficient in removing pathogens. However, they require more ecological footprint than any other wastewater treatment systems [6,7]. They are also less efficient in cold climates, require longer retention times, and significantly provide breeding areas for mosquitoes and other insects. Trickling filters are low-power facilities. They are simple and reliable. However, they are slow to adapt to environmental changes and experience regular clogging problems [8].

This is the author manuscript accepted for publication and has undergone full peer review but has not been through the copyediting, typesetting, pagination and proofreading process, which may lead to differences between this version and the [Version of Record](#).

Please cite this article as [doi: 10.1002/ceat.201700376](https://doi.org/10.1002/ceat.201700376)

This article is protected by copyright. All rights reserved.

MBRs have several advantages over the aforementioned conventional approaches such as small footprint and reactor requirements, high effluent quality, higher volumetric loading and less sludge production [9,10]. Conversely, MBRs experience reversible and irreversible fouling during filtration caused by the deposition of suspended or dissolved solids on the external membrane surface, on the membrane pores, or within the membrane pores [11,12]. Membrane fouling results in a decline in membrane performance. As a result, the membrane requires physical and chemical cleaning, hence increasing the cost of maintenance. EC reduces membrane fouling and prevents undesired heavy metal ions to be transferred into the treated wastewater [13,14].

The integration of EC with MBR in electrically-enhanced MBR (eMBR) would enhance the removal of pollutants and curtail membrane fouling. The coupling of electrokinetic treatment with MBR can enhance the removal of soluble organic materials, improve the performance characteristics of suspended solids such as dewaterability and filterability, and reduce MBR process constraints [15]. eMBR seems to provide very promising solutions and is becoming more attractive and increasingly integrated into wastewater treatment processes due to its high treatment efficiency, elimination of chemical addition for pretreatment and ease of control [13,16–20]. However, electricity cost and consumption of sacrificial electrode in eMBR still needs to be considered for performance improvements. This cost could be reduced if eMBR is operated at low current density and then, the treated effluent from eMBR is post-treated with inexpensive filters to remove residual contaminants. Residual organics, heavy metals, and microbes in treated wastewater effluents are harmful for potential end-use applications. The disposal of the treated effluents from eMBR containing these residual contaminants can also limit their end-use application to restricted reuse.

Therefore, a new approach that integrates a low-voltage eMBR with an inorganic ($\text{MnO}_2/\text{TiO}_2$) nanoporous membrane filter is proposed in this paper for enhanced wastewater treatment. Apart from the inherent physical adsorption characteristics of MnO_2 and TiO_2 ensured by their nanostructures, their capacities to achieve enhanced removal efficiencies of residual pollutants are compared in this paper. This approach is directed towards the production of a high-quality effluent at low cost. This proposed approach is original as per the authors' knowledge; no such integrated system has been developed or tested yet. The potential to incorporate this technology into existing wastewater treatment plants is investigated through the use of a real municipal wastewater as the feed to the integrated system.

2. Materials and methods

2.1. Materials

A continuous-mode eMBR testing facility was designed and fabricated. A polycomposite membrane having a pore size of $0.4\ \mu\text{m}$ and consisting of acrylonitrile butadiene styrene, polyethylene terephthalate, polypropylene and chlorinated polyethylene in the weight ratio 1:2:2:2 was inserted at the center of the eMBR, between two pairs of porous aluminum (25% porosity) anode and stainless steel cathode. The anode and cathode were placed at a distance of 5 and 10 cm, respectively, from the membrane. The feed was real municipal wastewater obtained from an MBR treatment plant having an operating capacity of 100,000 L/d. The

MnO₂ and TiO₂ nanoporous membranes were in the form of nanowire aerogels. The aerogels were fabricated as circular-disk filters having diameter of 47 mm. The fabrication procedures and properties of the aerogels have been reported in a recent paper by Kong's group [21]. These aerogels were characterized by 1D ultralong wires running up to several hundreds of micrometers with nanoscale diameters, high specific surface areas, and nanoporous channels. These characteristics are in addition to their low densities and thickness, and comparatively high tensile strain. The average nanowire diameters of the MnO₂ and TiO₂ were 15-20 nm and 50 nm, respectively. The specific surface area of the aerogels was 80 m²/g, which was almost close to the theoretical value. The young's modulus and tensile strengths of the aerogels were 25 and 1.1 MPa, respectively.

2.2. Integrated set-up of low-voltage eMBR and inorganic membrane

The food-to-microorganisms ratio in the eMBR was 0.59 1/d and current density was kept at 15 A/m² applied at a pulsed ON and OFF ratio of 1:3 every hour for 133 days. Sludge and hydraulic retention times of 240 and 13.5 h, respectively and a feed flow rate of 1.7 L/h were employed. A continuously stirred system is ensured by aerating the reactor content and pumping the wastewater and effluent into and out of the mixed liquor. The eMBR-inorganic membrane system is illustrated in Figure 2.1. The water contact angles of the inorganic membranes were measured by using KRÜSS Easy Drop contact angle analyzer with in-built drop shape analysis software. In addition, the nanowire morphology of the membranes was observed via FEI Nova NanoSEM 650 with monopole magnetic immersion final lens and 60⁰ objective lens geometry at an electron beam energy of 5 kV, 4.0 spot size, emission current of 100 μA, chamber vacuum < 10 mPa, and magnification of 500 nm. The treated effluent from eMBR was post-treated by filtering it through the inorganic membranes. Filtration through TiO₂ was carried out under UV illumination at the wavelength range of 315-400 nm and low intensity of 8 mW/cm². Filtration through MnO₂ membrane was carried out without UV light because of the weak photocatalytic response of MnO₂. The microbial (i.e. total bacterial count or TBC), organic (i.e. biological oxygen demand (BOD)), and heavy metal content (i.e. Cd²⁺, Fe²⁺, and Zn²⁺) in the final effluents from the integrated system were measured. The organic and heavy metal concentrations were obtained from HACH DR3900 UV/Vis spectrophotometer with radio-frequency identification (RFID) technology while the microbial contents of the effluents were measured using HACH m-ColiBlue24 Coliforms broth. The pollutant removal efficiencies, relative to the inorganic membranes, were obtained from Eq. (2.1).

$$R\% = 1 - (C_p/C_f) \quad (2.1)$$

R is membrane's removal efficiency for a particular pollutant; C_f is the concentration of the particular pollutant in eMBR effluent; C_p is the concentration of the pollutant in the final effluent obtained after filtration through the inorganic membranes.

The spectrophotometer used vials that have barcodes on them. Once a vial for a pollutant of interest was inserted inside the spectrophotometer, the device would read the barcode on the vial in order to set the maximum wavelength of UV/V is light that could be absorbed by the pollutant. The spectrophotometer measured the absorbance of UV/V is light by the pollutant

and converted the absorbance to a concentration parameter using the Beer's Law, as shown in Eq. (2.2).

$$A = \epsilon l c \quad (2.2)$$

A is absorbance; ϵ is molar absorptivity which is constant for the measured substance; l is the path length of the cuvette in which the sample is contained; c is the concentration. Chemical oxygen demand (COD) was first measured using HACH vial LCK 314. The percentage of BOD in the COD was then obtained from the oxygen uptake rate (OUR) method as 72.7%, as previously reported [22]. The photometric accuracy of the UV/Vis spectrophotometer was 1%. This photometric accuracy is the accuracy of the absorbance measured by the instrument, i.e. the error of the absorbance measured by the instrument was 1%. For the TBC measurements, 100 mL of sterile water was used as negative control. The positive control was 100 mL of sterile water spiked with commercial 5 μ L *E. Coli*. The sterile water was obtained by autoclaving deionized water using Tuttnauer Autoclave 2840 EL-D liquid mode. The analyzed samples included 100 mL of sterile water spiked with 100 μ L sewage, 10 mL eMBR treated effluent, 10 mL eMBR-MnO₂ treated effluent, and 10 mL eMBR-TiO₂ treated effluent. Each sample was filtered through the Whatman fritted glass filtration setup so that the bacteria in the sample can be collected on a cellulosic membrane (filter papers with pore size of 1.5 μ m and diameter of 47 mm). The media in the broth ampule were transferred onto two cellulose membranes which were firmly placed on each other inside a petri dish. Then, the cellulose membrane containing the bacteria was transferred face-up onto the content inside the petri dish. The petri dish was sealed with parafilm and incubated overnight at 37°C.

(Figure 2.1)

Changes in the chemical composition of the filters were also investigated through thermogravimetric analysis (TGA) and energy-dispersive X-ray spectroscopy (EDAX). TGA was carried out by using NETZSCH STA449 F3 Jupiter thermal analyzer in the temperature range of 24-950°C. 13 mg samples of the fresh and spent filters were thermally degraded in an aluminum pan crucible at a heating rate of 10°C/min and under nitrogen atmosphere with N₂ gas flow rate of 20 mL/min. EDAX was carried out via the Apollo X silicon drift detector in FEI Nova NanoSEM 650 at a working distance of 5 mm. The impact of surface charges on the removal of residual contaminants was also confirmed by dispersing the spent filters in deionized water, such that suspensions containing 0.04 mg/mL of MnO₂ and TiO₂ were obtained. The surface charges were determined from zeta potential measurements by using the phase analysis light scattering principle in NanoBrook ZetaPALS potential analyzer with a scattering angle of 15°. All measurements were carried out at room temperature (21 \pm 1°C).

3. Results and discussions

3.1 Removal efficiency of residual contaminants

eMBR alone showed good removal efficiency of the pollutants in wastewater, i.e. 99.5% TBC (from 3.195 million counts/100 mL to 18,300 counts/100 mL), 95.8% BOD removal (from 633.6 ppm to 26.8 ppm), 90% Fe^{2+} removal (from 281 ppb to 28 ppb), 78.8% Zn^{2+} removal (from 2.25 ppm to 476 ppb), and 79.4% Cd^{2+} removal (from 63 ppb to 13 ppb). However, these values are not low enough to make the eMBR treated effluent suitable for general and wholesome applications [23,24], hence the use of the eMBR-inorganic membrane integrated system was investigated. Water contact angle measurements showed that both filters were ultrahydrophilic; the filters exhibited complete wetting or water spreading with contact angle of 0° . The nanowire morphology of the inorganic membranes were confirmed via SEM imaging, as shown in Figure 3.1

(Figure 3.1)

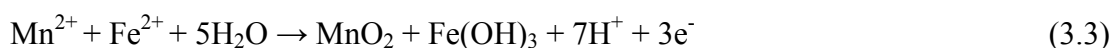
3.2 Heavy metal removal

MnO_2 membrane was able to reduce the concentrations of Fe^{2+} , Zn^{2+} , and Cd^{2+} in the eMBR effluent to 6, 451, and 10 ppb, respectively. On the other hand, the treated water obtained after filtration of eMBR effluent through TiO_2 membrane contained 28 ppb Fe^{2+} , 69 ppb Zn^{2+} , and 10 ppb Cd^{2+} . The relative contributions of eMBR, MnO_2 , and TiO_2 membrane to the removal of heavy metal ions can be observed from Table 3.1. Table 3.1 shows the concentrations of heavy metal ions in the wastewater, eMBR, and inorganic membranes.

(Table 3.1)

3.2.1 Fe removal

The MnO_2 membrane was able to further reduce the Fe content of the eMBR treated effluent from 28 ppb to 6 ppb (78.6% relative removal efficiency). Fe is mainly present as dissolved or ferric (Fe^{2+}) ions in water at alkaline pH. At the pH of eMBR treated effluent (pH of 8.03), the chemical oxidation of Fe^{2+} to insoluble ferrous ions (Fe^{3+}) was achieved through the top layer of the oxidizing MnO_2 surface. During filtration, the Fe^{2+} ions were chemisorbed on the MnO_2 surface in such a way that the dissolved Fe^{2+} ions were oxidized to Fe^{3+} whereas the free Mn^{2+} ions displaced from the surface of the media were reduced as a result of alkaline hydrolysis and became converted chemically to the surrounding MnO_2 [25,26]. These mechanisms can be represented by Eq. (3.1)-(3.3).



In the case whereby the treated effluent is at acidic pH, the alkalinity needs to be adjusted before MnO_2 filtration can occur because the process would be deterred by the protonation or solubilization of the oxidized Mn^{2+} and the active sites of the surrounding MnO_2 in water. Also, at lower pH, Fe^{2+} would compete with H^+ or H_3O^+ for the binding sites and subsequently, the surface of the MnO_2 filter would become positively charged and its adsorption efficiency for Fe^{2+} would be adversely affected [27]. However, for this study, the treated effluent was at a slightly alkaline pH. At this pH, the H^+ ions produced were eventually neutralized to water because of deprotonation arising from the presence of the excess OH^- ions in water. The insoluble Fe^{3+} ions obtained in the form of $\text{Fe}(\text{OH})_3$ became suspended in water and were removed by precipitation and then filtered out on the surface of the MnO_2 media during filtration. The TiO_2 filter showed no response and surface interaction with Fe^{2+} , possibly because of the competition of other ions and organics for the illuminated surface.

3.2.2 Cd and Zn removal

The MnO_2 filter was able to reduce Cd concentration in the eMBR treated effluent from 13 ppb to 10 ppb (i.e. 23% relative removal efficiency), and Zn concentration from 476 ppb to 451 ppb (i.e. 5.3% relative removal efficiency). In general, the removal efficiency of the filter was in the following order: $\text{Fe} > \text{Cd} > \text{Zn}$. This might be due to the differences in the electronegativity and sizes of the dissolved ions of these metals [28]. Ideally, the electronegativity of the metallic ions varies inversely with their size because of the reduced attraction between the electrons in their valence band and the positively charged nucleus. As electronegativity is the tendency of matter to attract electrons or become reduced, the reduction of the metal ions was in line with the order of their electronegativity (i.e. electronegativity of $\text{Fe} > \text{Cd} > \text{Zn}$) and inversely related to their sizes (i.e. size of $\text{Zn} > \text{Cd} > \text{Fe}$). The initial concentration of the heavy metals also played an important role in their removal. For example, the absolute removal of Zn (25 ppb) was more than that of Cd (0.3 ppb) because of the availability of more ions to occupy and saturate more binding sites of the nanowires [29].

The metal ions were transferred to the adsorbed surface through the complex mechanisms of external mass transfer, film and intraparticle diffusion, and eventual chemical bonding [30]. The film and intraparticle diffusion mechanisms were controlled by the sizes of the heavy metal ions which were larger than the pores of the membrane filters. At the slightly alkaline pH of the eMBR treated effluent, the electrostatic interaction between the negatively charged active sites of the filters and positively charged metallic ions also contributed to the removal of these ions, apart from the physical retention offered by the nanoporous channels. $\alpha\text{-MnO}_2$ is an acidic oxide containing a negatively charged surface that can enhance its capacity to adsorb dissolved positively charged metal ions in water at alkaline pH [31]. Cd^{2+} was precipitated as $\text{Cd}(\text{OH})^+$, $\text{Cd}(\text{OH})_2$ and finally $\text{Cd}(\text{OH})_3$; and Zn^{2+} was precipitated as $\text{Zn}(\text{OH})^+$, $\text{Zn}(\text{OH})_2$ and finally $\text{Zn}(\text{OH})_3$ [27]. The same mechanisms can be proposed for the removal of Cd and Zn by TiO_2 . The relative removal efficiency of TiO_2 for Cd is the same as that of MnO_2 , i.e. TiO_2 was also able to reduce the Zn content in eMBR treated effluent from 13 ppb to 10 ppb. However, TiO_2 displayed higher removal efficiency for Zn (from 476 ppb to 69 ppb) possibly because of the affinity of Zn^{2+} ion to be adsorbed to multiple coordinated sites at the water- TiO_2 interface arising from steric hindrance effects [32].

3.2.3 Bacteria and BOD

E. Coli appeared on the media as blue colonies while other coliforms (*Fecal Coliforms*) appeared as red colonies. These colonies were counted and their sum gave the TBC. TiO₂ showed excellent removal efficiency for bacteria. The TiO₂ filter was able to achieve 100% removal of the residual TBC from the eMBR treated effluent, even at the very low UV illumination of 8 mW/cm² for 30 min. The high removal efficiency obtained might not be unconnected with the anatase nanowire structure. As the filter was illuminated, the excitation of electrons from the valence band to the conduction band occurred, which resulted in the production of paired positive hole and negative electron on the TiO₂ surface. The ultralong nanowires might have enhanced the motion of the photogenerated electron-hole pair, such that the kinetics of degradation of biological matter on the TiO₂ surface was promoted. Although the band gap of the TiO₂ (3.2 eV) is closer to the UV spectrum, the nanowire anatase crystallite structure promoted its photocatalytic capacity [33]. The electron-hole pair reacted with oxygen and adsorbed water to produce O₂•⁻ or •OH as products [34], as shown in Eq. (3.4)–(3.7).



$h\nu$ is the photon energy. OH• is the main reactive oxygen specie in the photocatalytic action of TiO₂ [35]. These reactive oxygen species might have influenced the lysis or endogenous respiration of the outer membranes and cellular components of the residual bacteria in the treated effluent [35]. However, MnO₂ showed 0% removal of bacteria. Rather, bacterial growth was enhanced by the MnO₂ filter. MnO₂ was able to increase the TBC of the eMBR treated effluent from 18,300 counts/100 mL to 98,000 counts/100 mL. This strange occurrence might be due to the non-photocatalytic influence of the MnO₂ membrane and the alkaline pH of filtration that restricted the solubilization of the MnO₂ surface or its oxidizing capability. It is possible that there were some manganese-precipitating cells in the eMBR treated effluent, which might have influenced bacterial growth on the MnO₂ surface placed on the filter holder [36]. Similarly, TiO₂ showed better removal efficiency of the residual BOD than MnO₂ because of the same reasons. TiO₂ and MnO₂ were able to reduce the BOD content of the eMBR effluent from 26.8 ppm to 13.7 ppm and 15.3 ppm, respectively. The improved retention and degradation of residual organics by TiO₂ was further confirmed by the zeta potential measurements. It was observed that the surface of the spent TiO₂ was more negatively charged than that of MnO₂. Consequently, the conductance of the TiO₂ surface was higher (270 μS, against 145 μS for the spent MnO₂). Hence, the TiO₂ surface required more current to sustain charge mobility under an electric field of ~ 15 V/cm. The zeta potentials of the spent TiO₂ and MnO₂ surfaces were -29.76 mV and -8.82 mV, respectively. These surfaces required electric current of 1.57 mA and 0.90 mA, respectively to sustain the mobility of the surface charges under the influence of electric field.

3.2.4 Applicability of the eMBR-nanowire system

The potential applications for all treated effluents are summarized in Table 3.2. Restricted reuse involves infrequent and controlled public exposure such as landscaping, forestry irrigation, and artificial recharge etc. General reuse involves frequent and uncontrolled public exposure such as agricultural irrigation, car washing, district cooling, industrial process heating/cooling etc. Meanwhile, the regenerative potential of the inorganic membranes is quite critical for these applications. It was observed that physical desorption alone might not be sufficient for the regeneration of the filters. Chemical cleaning solutions might be needed for the removal of chemisorbed contaminants and complete regeneration of the filters. This is a crucial limitation of the use of the filters for the removal of residual contaminants from treated wastewater effluent.

(Table 3.2)

The physically retained precipitates were washed away during desorption whereas the chemically bonded metal ions and residual organics (which were not degraded by photocatalysis, in the case of TiO_2) remained on the membranes after desorption, as revealed by EDAX (Figure 3.2 (a),(b)). The differences between the elemental compositions of the fresh and spent membrane filters are shown in Table 3.3.

(Figure 3.2)

(Table 3.2)

The EDAX measurements were confirmed through TGA. From the thermographs (Figure 3.3), the spent filters showed higher thermal decomposition rates than their fresh counterparts because of the attachment of some organics and new functional groups to the initial inorganic oxide functionality.

(Figure 3.3)

For the fresh MnO_2 filter, the first weight loss occurred at a temperature of up to 104°C , possibly due to the release of water of hydration that was not completely removed from its hydrogel. The second weight loss occurred up to 240°C leading to 76% total weight loss, due to the degradation and dissociation of oxygen from MnO_2 . At $\sim 300^\circ\text{C}$, 13 mg of the fresh MnO_2 filter has been completely burned out. For the spent MnO_2 filter, steeper slopes were observed; the short slope close to $\sim 100^\circ\text{C}$ may represent the release of physically adsorbed water (about 11%). Thereafter, a very steep degradation of the spent filter was noticed up to $\sim 168^\circ\text{C}$ due to the endothermic dissociation of the organics, adsorbed precipitates and partly collapsed nanowire network [37]. 13 mg of the spent filter was completely degraded at 168°C .

The fresh TiO_2 showed two regions – release of 18% of water of hydration up to 23°C and a second step indicating a total weight loss of about 40% (that continued up to 950°C) due to steady degradation of the crystal structure. The thermograph of the spent TiO_2 filter showed three distinct and steeper steps, i.e. release of about 32% of bound water and hydroxyl groups up to 107°C ; elimination of inorganic precipitates, adsorbed organics and residuals of photocatalytically-degraded organics at $107\text{--}235^\circ\text{C}$ [38]; and considerable weight loss at $235\text{--}300^\circ\text{C}$, indicating no crystallization or phase transition [39]. Complimentarily, the EDAX spectra of the spent filters show more intense peaks than those of the fresh filters, indicating the attachment of residual contaminants to the filters.

4. Conclusions

Nanoporous MnO_2 and TiO_2 membranes were used for the removal of residual contaminants from treated wastewater effluent. These membranes contain ultralong 1D nanowires and nanoporous channels. The MnO_2 and TiO_2 nanowires have chemical functionalities for membrane separation and photocatalytic ability. MnO_2 displayed a better capacity to remove Fe^{2+} because its negatively charged surface was able to take out Fe^{2+} ions as Fe^{3+} precipitate. On the other hand, TiO_2 displayed higher removal efficiency for Zn^{2+} because there were multiple coordinated sites at the water- TiO_2 interface, due to the greater surface area of the TiO_2 membrane per unit mass. Both materials displayed the same removal efficiency for Cd^{2+} . Meanwhile, TiO_2 showed enhanced removal efficiency for BOD and bacteria. The 1D nanowire morphology was shown to improve the capacity of TiO_2 to absorb and scatter light as a result of the high length-to-diameter ratios offered by this morphology, such that the in-situ photogenerated electron-hole pairs can be moved to the adsorbed organics within the conduction band. The final treated effluents obtained from the eMBR- MnO_2 and eMBR- TiO_2 systems are suitable for general and restricted applications. However, the regeneration of the filters by physical desorption is not feasible. Membrane fouling due to chemisorption and electrostatic interaction might be a challenge during long-term operation. Further research needs to be directed towards the development of solvents and organic chemicals that can ensure “green” regeneration of the MnO_2 and TiO_2 . In addition, MnO_2 is not feasible for bacteria removal while TiO_2 is unsuitable for Fe removal. For advanced water reuse such as wholesome or near-potable applications, the integration of both materials in eMBR- MnO_2 - TiO_2 configuration might be able to address these challenges.

Acknowledgment

This work was funded by the Cooperative Agreement between the Masdar Institute of Science and Technology (Masdar Institute), Abu Dhabi, UAE and the Massachusetts Institute of Technology (MIT), Cambridge, MA, USA - Reference 02/MI/MIT/CP/11/07633/GEN/G/00. Authors declare no conflict of interest.

References

- [1] M. K. H. Winkler, R. Kleerebezem, M. C. M. Van Loosdrecht, *Water Res.* **2012**, *46*, 136. <https://doi.org/10.1016/j.watres.2011.10.034>
- [2] I. Kim, D.-C. Choi, J. Lee, H.-R. Chae, J. Hee Jang, C.-H. Lee, P.-K. Park, Y.-J. Won, *J. Memb. Sci.* **2015**, *490*, 190. <https://doi.org/10.1016/j.memsci.2015.04.026>
- [3] G. Chen, *Sep. Purif. Technol.* **2004**, *38*, 11. <https://doi.org/10.1016/j.seppur.2003.10.006>
- [4] W. Q. Guo, S. S. Yang, W. S. Xiang, X. J. Wang, N. Q. Ren, *Biotechnol. Adv.* **2013**, *31*, 1386. <https://doi.org/10.1016/j.biotechadv.2013.06.003>
- [5] S. S. Yang, W. Q. Guo, Z. H. Meng, X. J. Zhou, X. C. Feng, H. S. Zheng, B. Liu, N. Q. Ren, Y. S. Cui, *Bioresour. Technol.* **2013**, *131*, 560. <https://doi.org/10.1016/j.biortech.2013.01.024>
- [6] C. Grady Jr, G. Daigger, N. Love, C. Filipe, CRC Press, **2011**.
- [7] A. K. Kivaisi, *Ecol. Eng.* **2001**, *16*, 545. [https://doi.org/10.1016/S0925-8574\(00\)00113-0](https://doi.org/10.1016/S0925-8574(00)00113-0)
- [8] O. I. Lekang, H. Kleppe, *Aquac. Eng.* **2000**, *21*, 181. [https://doi.org/10.1016/S0144-8609\(99\)00032-1](https://doi.org/10.1016/S0144-8609(99)00032-1)
- [9] J. Hoinkis, S. A. Deowan, V. Panten, A. Figoli, R. R. Huang, E. Drioli, in *Procedia Eng.*, **2012**, pp. 234–241. <https://doi.org/10.1016/j.proeng.2012.01.1199>
- [10] J. Radjenovic, M. Matosi, I. Mijatovic, M. Petrovic, D. Barcelo, *Membrane Bioreactor (MBR) as an Advanced Wastewater Treatment Technology*, Springer Berlin Heidelberg, Berlin, Heidelberg, **2008**. <https://doi.org/10.1007/978-3-540-79210-9>
- [11] N. S. A. Mutamim, Z. Z. Noor, M. A. A. Hassan, G. Olsson, *Desalination* **2012**, *305*, 1. <https://doi.org/10.1016/j.desal.2012.07.033>
- [12] L. Liu, J. Liu, B. Gao, F. Yang, S. Chellam, *J. Memb. Sci.* **2012**, *394–395*, 202. <https://doi.org/10.1016/j.memsci.2011.12.042>
- [13] S. W. Hasan, M. Elektorowicz, J. A. Oleszkiewicz, *Chemosphere* **2014**, *97*, 71. <https://doi.org/10.1016/j.chemosphere.2013.11.009>
- [14] E. Abdulkarem, I. Ahmed, M. R. M. Abu-Zahra, S. W. Hasan, *Desalination* **2017**, *403*, 107. <https://doi.org/10.1016/j.desal.2016.06.004>
- [15] S. Ibeid, M. Elektorowicz, J. A. Oleszkiewicz, *Water Res.* **2013**, *47*, 6358. <https://doi.org/10.1016/j.watres.2013.08.007>
- [16] A. Giwa, S. Daer, I. Ahmed, P. Marpu, S. Hasan, *J. Water Process Eng.* **2016**, *11*, 88. <https://doi.org/10.1016/j.jwpe.2016.03.011>
- [17] S. W. Hasan, M. Elektorowicz, J. A. Oleszkiewicz, *Bioresour. Technol.* **2012**, *120*, 199. <https://doi.org/10.1016/j.biortech.2012.06.043>
- [18] A. Giwa, S. W. Hasan, *J. Environ. Manage.* **2015**, *164*, 1. <https://doi.org/10.1016/j.jenvman.2015.08.031>
- [19] A. Giwa, I. Ahmed, S. W. Hasan, *J. Environ. Manage.* **2015**, *159*, 78. <https://doi.org/10.1016/j.jenvman.2015.05.035>
- [20] S. W. Hasan, I. Ahmed, A. A. Housani, A. Giwa, *Sci. Rep.* **2016**, *6*, 31828. <https://doi.org/10.1038/srep31828>
- [21] S. M. Jung, H. Y. Jung, W. Fang, M. S. Dresselhaus, J. Kong, *Nano Lett.* **2014**, *14*, 1810. <https://doi.org/10.1021/nl404392j>
- [22] A. Giwa, Modelling and experimental investigation of membrane bio-electro-reactor (MBER) for Masdar city wastewater treatment, M. Sc. Thesis, Masdar Institute of Science and Technology, Abu Dhabi, United Arab Emirates., 2014.
- [23] Regulation and Supervision Bureau (RSB), *Water Quality Regulations*, Regulations

- And Supervision Bureau, Abu Dhabi, United Arab Emirates, **2013**.
- [24] U.S. Environmental Protection Agency, *Guidelines for Water Reuse*, **2004**.
- [25] C. Noubactep, K. B. D. Btatek, J. B. Tchatchueng, *Chem. Eng. J.* **2011**, 178, 78.
<https://doi.org/10.1016/j.cej.2011.10.014>
- [26] Nobel service, *Technical Information: Iron Removing*, Milan, Italy, **2016**.
- [27] Z. Zhu, H. Ma, R. Zhang, Y. Ge, J. Zhao, *J. Environ. Sci.* **2007**, 19, 652.
[https://doi.org/10.1016/S1001-0742\(07\)60109-0](https://doi.org/10.1016/S1001-0742(07)60109-0)
- [28] W. S. Wan Ngah, M. A. K. M. Hanafiah, *Bioresour. Technol.* **2008**, 99, 3935.
<https://doi.org/10.1016/j.biortech.2007.06.011>
- [29] R. Balasubramanian, S. V. Perumal, K. Vijayaraghavan, *Ind. Eng. Chem. Res.* **2009**, 48, 2093. <https://doi.org/10.1021/ie801022p>
- [30] C. Luo, R. Wei, D. Guo, S. Zhang, S. Yan, *Chem. Eng. J.* **2013**, 225, 406.
<https://doi.org/10.1016/j.cej.2013.03.128>
- [31] S. Bajpai, M. Chaudhuri, *J. Environ. Eng.* **1999**, 125, 782.
[https://doi.org/10.1061/\(ASCE\)0733-9372\(1999\)125:8\(782\)](https://doi.org/10.1061/(ASCE)0733-9372(1999)125:8(782))
- [32] G. He, G. Pan, M. Zhang, G. A. Waychunas, *Environ. Sci. Technol.* **2011**, 45, 1873.
<https://doi.org/10.1021/es1035283>
- [33] T. Luttrell, S. Halpegamage, J. Tao, A. Kramer, E. Sutter, M. Batzill, *Sci. Rep.* **2014**, 4,
<https://doi.org/10.1038/srep04043>
- [34] A. H. Jawad, N. S. A. Mubarak, M. A. M. Ishak, K. Ismail, W. I. Nawawi, *J. Taibah Univ. Sci.* **2016**, 10, 352. <https://doi.org/10.1016/j.jtusci.2015.03.007>
- [35] U. Joost, K. Juganson, M. Visnapuu, M. Mortimer, A. Kahru, E. Nõmmiste, U. Joost, V. Kisand, A. Ivask, *J. Photochem. Photobiol. B Biol.* **2015**, 142, 178.
<https://doi.org/10.1016/j.jphotobiol.2014.12.010>
- [36] K. H. Nealson, J. Ford, *Geomicrobiol. J.* **1980**, 2, 21.
<https://doi.org/10.1080/01490458009377748>
- [37] A. Zolfaghari, H. R. Naderi, H. R. Mortaheb, *J. Electroanal. Chem.* **2013**, 697, 60.
<https://doi.org/10.1016/j.jelechem.2013.03.012>
- [38] S.-H. Wang, K.-H. Wang, Y.-M. Dai, J.-M. Jehng, *Appl. Surf. Sci.* **2013**, 264, 470.
<https://doi.org/10.1016/j.apsusc.2012.10.046>
- [39] K. V. Bineesh, D.-K. Kim, D.-W. Park, *Nanoscale* **2010**, 2, 1222.
<https://doi.org/10.1039/c0nr00108b>